

SYNTHETIC JETS IN CROSS-FLOW

PART I: ROUND JET

K. B. M. Q. Zaman^{*}
National Aeronautics and Space Administration
Glenn Research Center
Cleveland, OH 44135

Ivana M. Milanovic[†]
University of Hartford
West Hartford, CT 06117

ABSTRACT

Results of an experimental investigation on synthetic jets from round orifices with and without cross-flow are presented. Jet Reynolds number up to 46,000 with a fully turbulent approach boundary layer, and Stokes number up to 400, are covered. The threshold of ‘stroke length’ for synthetic jet formation, in the absence of the cross-flow, is found to be $L_0/D \approx 0.5$. Above $L_0/D \approx 10$, the profiles of normalized centerline mean velocity appear to become invariant. It is reasoned that the latter threshold may be related to the phenomenon of ‘saturation’ of impulsively generated vortices. In the presence of the cross-flow, the penetration height of a synthetic jet is found to depend on the ‘momentum-flux ratio’. When this ratio is defined in terms of the maximum jet velocity and the cross-flow velocity, not only all data collapse but also the jet trajectory is predicted well by correlation equation available for steady jets-in-cross-flow. Distributions of mean velocity, streamwise vorticity as well as turbulence intensity for a synthetic jet in cross-flow are found to be similar to those of a steady jet-in-cross-flow. A pair of counter-rotating streamwise vortices, corresponding to the ‘bound vortex pair’ of the steady case, is clearly observed. Mean velocity distribution exhibits a ‘dome’ of low momentum fluid pulled up from the boundary layer, and the entire domain is characterized by high turbulence.

NOMENCLATURE

A	RMS voltage input to loudspeaker
D	Orifice diameter (in)
f	Forcing frequency (Hz)
J	Momentum-flux ratio, $J = (V_{max}/U_{\infty})^2$

L_0	Stroke length, $L_0 = \int_0^{T/2} v_o(t) dt$
Re	Reynolds number, $Re = \bar{V}D/\nu$, $\bar{V} = 2V_0$
S	Stokes number, $S = \sqrt{2\pi f D^2/\nu}$
t	Time
T	Forcing period, $T = 1/f$
V_0	Velocity during discharge phase of the cycle averaged over entire period, $V_0 = \frac{L_0}{T} = f \int_0^{T/2} v_o(t) dt$
\bar{V}	Average velocity during discharge phase of the cycle
V_{max}	Maximum velocity during discharge phase
$v_o(t)$	Velocity at exit center of orifice (at $x = y = z = 0$)
U, V, W	Mean velocity in streamwise, normal and spanwise directions
u', v', w'	Turbulence intensity in streamwise, normal and spanwise directions
x, y, z	Cartesian coordinates in streamwise, normal and spanwise directions (Fig. 1)
y_{max}	Jet penetration denoted by location of u'_f -peak
ν	Kinematic viscosity

SUBSCRIPTS

c	Centerline
f	Fundamental amplitude at forcing frequency
j	Jet
∞	Cross-stream

^{*} Associate Fellow AIAA, Aerospace Engineer

[†] Member AIAA, Assistant Professor

INTRODUCTION

Active flow control for enhancing propulsive and aerodynamic performance of an aircraft, over a wide range of operating conditions, is of considerable current interest. Potential benefits include alleviation of separation in inlets and ducts, stall margin improvement for turbomachinery, mixing enhancement in jet exhausts and combustors, lift enhancement and drag reduction for wings as well as noise reduction. Most flow control techniques such as vortex-generating-jets, steady or pulsed suction, bleed and oscillatory blowing require a fluid source and accompanying support hardware. In recent research synthetic jets have emerged as a promising technique since they introduce flow perturbation without a net mass injection. Thus, there is no requirement for bleed fluid and minimal demand for additional hardware.

A synthetic jet is created from the ambient fluid by impressing an oscillating pressure gradient across an orifice. Suction pressure entrains the fluid into the orifice, and during the discharge phase flow separates at the edges forming a shear layer. The vortex sheet then rolls up and advects away under its own induced velocity. Consequently, a net momentum is transferred to the surrounding fluid even though the net mass flux is zero. Discrete vortical structures found near the jet exit develop instability followed by vortex core breakdown and the emergence of a fully developed turbulent jet.¹

A synthetic jet can be generated by a cavity-membrane configuration attached to the jet orifice. Forced oscillatory motion of the membrane, placed on a surface of the cavity, imposes the oscillatory pressure on the orifice. This results in the alternating entrainment and ejection from the orifice causing the formation of the synthetic jet. The pertinent phenomenon of acoustics generating a flow in the presence of a solid surface, or ‘acoustic streaming’, has been well known and studied by aeroacousticians in the past^{2,3} as well as lately.⁴ Recent research, e.g. of Ref. 1, and many others cited in the following, have illustrated the potential of this phenomenon to be a useful flow control tool.

Numerous studies addressed the fundamentals and potential application of synthetic jets. We touch upon only a few, and the list is by no means exhaustive. Several experiments have noted the resemblance of synthetic jets to continuous jets,^{1,5-7} and direct comparison at same Reynolds number^{8,9} confirmed self-similar velocity profiles in the asymptotic regions. However, in the initial development region the synthetic jets have been found to grow both in width and volume flux more rapidly due to the

vigorous vortical structures. When applied to flows in various propulsion components synthetic jets have been shown to produce many beneficial effects.⁸⁻¹⁷ Specifically, they have been demonstrated to improve lift and drag of bluff bodies,¹⁴ produce desirable vectoring effects on primary jets,¹³ delay stall on airfoils,⁸ enhance fuel-air mixing,¹⁵ reduce losses and increase the volume flow rate in internal duct flow,¹⁶ and diminish blade vortex interaction noise.¹⁷ There are ongoing efforts to achieve high amplitude perturbations from compact and rugged designs so that the technique could be brought closer to practical application.¹⁸⁻²⁰

In terms of basic research, while extensive work has been done on the structure and dynamics of a synthetic jet, its behavior in a cross-flow has been addressed in relatively few investigations. Virtually all applications would involve a cross-flow that is to be ‘controlled’. Also, while round or rectangular orifices were the subject of previous studies, in applications the orifice geometry could often be complex involving pitch and yaw and cluster of orifices. Data for such configurations are not readily available. Furthermore, detailed flowfield information including vorticity and turbulent stresses, useful for simulation and development of models, are also lacking. Finally, most previous works involved relatively low Reynolds number jets, as noted in Ref. 7, and an exploration at higher Re was deemed appropriate. These provided the motivation for a further investigation.

In the current investigation, wind tunnel experiments are carried out using hot-wire anemometry. The synthetic jet (referred in the following as SJ) is produced by a cavity-loudspeaker combination. The characteristics of the SJs, from orifices of different geometry, with and without the cross-flow, are studied. In view of the volume and scope of the results, we present them in two parts. In this part, the behavior and parametric dependence of a basic SJ and a synthetic jet in cross-flow (referred in the following as SJCF) are discussed. In the second part, SJCF from orifices of different geometry are compared with a detailed documentation of the flowfields.

EXPERIMENTAL SETUP

The experiments were conducted in a NASA GRC low speed wind tunnel with 30 x 20 in test section. Synthetic jets were created by a loudspeaker (Altec Lansing 16 in. woofer) housed in a chamber underneath the test section as shown in Fig. 1. Most of the data for round jets pertain to the orifice diameter, $D = 0.75$ in. Limited data were obtained for diameters of 0.375, 1.5 and 3 in. For the results presented in Part 1, the orifices were straight holes cut through a clear plastic disc of 1-in. thickness. The disc was mounted flush on the test section floor.

In order to obtain highest sound pressure amplitudes Helmholtz resonance of the chamber was utilized. However, off-resonance frequencies were frequently used when requiring smaller amplitudes. The resonance frequencies for $D = 0.75$ and 3.0 in. orifices, for example, were calculated to be 27.6 and 76.7 Hz, respectively. These were confirmed by amplitude measurement at the exit while varying the frequency. The resonant frequency increased somewhat when the cross-flow was turned on, in agreement with previous observations.²¹ For a given frequency, the amplitude of the pulsatile flow was controlled by varying the input voltage, A , to the woofer.

The measurements were performed by standard hot-wire anemometry. Two \times -wires, one in ' $u-v$ ' and the other in ' $u-w$ ' configuration, were used for flow mapping in the cross-flow plane. The probes were stepped through the same grid points allowing the measurement of all three components of mean velocity and turbulence intensity. A single element of the ' $u-w$ ' wire, with appropriate calibration, was used to measure the velocity characteristics at the exit of the orifice. The origin of the coordinate system is located at the center of the orifice as illustrated in Fig. 1. The streamwise or cross-stream direction (parallel to the tunnel flow) is denoted by x , the direction normal to the tunnel floor is denoted by y , and the spanwise direction along the tunnel floor by z .

Most of the measurements with the SJCF were done for a cross-stream velocity of $U_\infty = 20$ ft/s. The approach boundary layer was turbulent with a thickness about 60% of the orifice diameter as seen in Fig. 2. Turbulence intensity measurements at a fixed location are also shown in Fig. 2. These data indicate that the boundary layer transitions around $U_\infty = 12$ ft/s. All results presented are for higher values of U_∞ so that the approach boundary layer was fully turbulent.

RESULTS

Time traces from the single hot-wire are shown in Fig. 3 for various vertical locations on the axis of the orifice, without the cross-flow ($U_\infty = 0$). For illustration purposes the traces are staggered successively by one major ordinate division. Near the orifice, flow is reversed during the suction half of the cycle. Velocity readings however are positive throughout the cycle due to the directional insensitivity of the hot-wire. The 'rectification' is clearly seen at $y/D = 0.2$ where the part of the cycle involving smaller amplitudes represents the reverse suction flow. With increasing axial distance the signal during the discharge part of the cycle becomes dominant. The rectification is practically gone at $y/D = 0.5$, and the velocity is positive everywhere at $y/D = 1.0$. The hot-wire rectification is no longer a

problem somewhat above the orifice ($y/D > 1.0$) and farther downstream ($x/D > 1.0$) with the cross-flow on. As elaborated below, the hot-wire trace from the discharge phase, measured at the smallest y , is utilized to calculate the characteristic velocity, V_0 .

The properties of the SJ were determined using Smith and Glazer's¹ definition:

$$V_0 = \frac{L_0}{T} = f \int_0^{T/2} v_0(t) dt, \quad (1)$$

where V_0 , the characteristic velocity, is the integrated value over the discharge half of the cycle and averaged over the entire period. The stroke length, L_0 , is the equivalent length of a slug of fluid discharged during the relevant half of the cycle. In order to evaluate V_0 and L_0 the time traces were phase-averaged using the signal to the loudspeaker as reference.

Figures 4(a) and 4(b) illustrate sample phase-averaged traces for the probe location of $y/D = 0.2$ and $z/D = 0$. Results are shown for (a) various radial locations, x/D , without the cross-flow, and (b) the exit center while varying U_∞ . It can be seen in Fig. 4(a) that the traces are practically identical for different radial locations and deviation occurs only when the probe is drawn close to the edge of the orifice. The larger peak on the right indicates the discharge half of the cycle. The peak amplitude of the trace during this half together with the trough in the middle are utilized to estimate V_0 and L_0 , assuming a sinusoidal function. The quantities V_0 and L_0 obtained in this manner for representative cases of the study are listed in Table 1. With the onset of the cross-flow, in Fig. 4(b), only small changes have taken place during the rising portion of the signal. Integration of the velocity over the discharge phase made only minor difference in the value of V_0 with and without the cross-flow. Thus, for the range of U_∞ covered, V_0 and L_0 remain practically unchanged for a given frequency and amplitude, and the parameters listed in Table 1 pertain to cases both with and without the cross-flow.

Normalized centerline velocity profiles without the cross-flow are presented in Fig. 5. Mostly due to hot-wire rectification a positive velocity is read erroneously near the exit, and the data for $y/D < 1$ are disregarded for the rest of the discussion. Clearly, there is a limiting value of L_0/D at which the velocity profile shows an initial peak and subsequent decay, such as in case 13. Cutoff stroke length is approximately $L_0/D = 0.5$, and below this threshold a synthetic jet is not formed. The velocity away from the orifice quickly drops to zero, as in case 16.

The observed threshold for jet formation agrees with a criterion,

$$\frac{Re}{S^2} > K, \quad (2)$$

developed by Utturkar et al.⁴ From experimental data for axisymmetric synthetic jets the threshold K was found to be about 0.16. In terms of the stroke length, this can be expressed as:

$$\frac{L_0}{D} > \pi K \quad (3)$$

The inequality (3), with the given value of K , yields a L_0/D threshold of about 0.5. Thus, the current data are in excellent agreement with the observations of Ref. 4. Stokes (S) and Reynolds (Re) numbers covered in earlier experiments^{2,4,22} spanned from very low values up to 110 and 5000, respectively. In the present work, much higher ranges are covered (Table 1). Note that Re in this study is based on \bar{V} , in order to be consistent with the notation of Ref. 4, so that the threshold of Eq. (2) could be compared directly. If V_0 were used as velocity scale, as in some previous studies, Re values listed in Table 1 would be halved.

A systematic trend in the profiles of Fig. 5 is also observed with increasing L_0/D . The peak velocity decreases progressively, and at large L_0/D the profiles settle down with very little further change. Compare the cases 4, 7 and 8. Thus, there appears to be an upper threshold, $L_0/D \approx 10$, above which the normalized centerline velocity profiles become invariant. This is further illustrated in Fig. 6. The amplitudes of the peaks from Fig. 5 are plotted as a function of L_0/D . The amplitudes drop with increasing L_0/D and levels off when $L_0/D > 10$.

It is possible that the upper threshold may have a connection to an observation of Gharib et al.²³ In that work impulsively generated vortex rings with a piston and cylinder arrangement were studied in a water tunnel. Circulation on one half of the cross sectional plane containing the jet axis was measured. The total circulation introduced in the flow was a direct function of the piston displacement that is equivalent to the stroke length in the present nomenclature. For small L_0/D the total circulation equaled that in the rolled up vortex. However, with increasing L_0/D , above a certain level, the circulation within the vortex became invariant. For large L_0/D , the excess circulation imparted to the flow appeared as lumps of vorticity trailing the primary vortex. The connection of this observation to the synthetic jets may be as follows.

The synthetic jet is generated mainly due to the induced velocity of the primary vortex. The effect of the fragmented trailing vortices is expected to be only secondary. Thus, if the strength of the primary vortex remains unchanged with increasing L_0/D little further strengthening of the SJ may be expected. This might explain the behavior observed at high L_0/D in Figs. 5 and 6. However, the threshold in Ref. 23 is approximately $L_0/D = 4$. This differs from the value of about 10 found for the synthetic jets in the current study. It is not clear if the disparity stems from a difference in the dynamics of an isolated vortex ring and those of periodic vortex rings involved in the synthetic jet. One notes, however, that Reynolds numbers in the present work are much higher compared to those of Ref. 23. In fact, within the range covered, data at higher Re in Ref. 23 exhibited trends that suggest a threshold of L_0/D above 4. It is not clear, however, if a Re dependence would explain the difference, and if indeed the connection stated above is valid. A full understanding will require further investigation.

Data for the synthetic jet with the cross-flow are now presented. Vertical profiles measured five diameters downstream from the orifice are shown in Fig. 7. These data are for a forcing frequency of 25 Hz, cross-stream velocity of 20 ft/s, and various amplitudes, A . The stroke lengths and corresponding case numbers of Table 1 are indicated in the legends. Profiles of mean velocity (U) are shown in Fig. 7(a). Corresponding turbulence intensity (u') and fundamental intensity (u'_f) data are shown in Figs. 7(b) and (c), respectively. A step-like behavior is developed in the U -distributions with increasing L_0/D . The turbulence u' remains high throughout the region of lower U and drops off sharply as U approaches U_∞ . The u'_f data were obtained via spectral analysis of the hot-wire signal. The drop-off in u' coincides with the occurrence of a peak in the u'_f -profile. The location of the u'_f -peak, denoted as y_{max} , provides a measure of the penetration for the SJCF. Note that with increasing L_0/D the height y_{max} increases. That is, the penetration of the SJCF increases with larger stroke length. Additional profiles of the fundamental intensity only for various combinations of forcing frequency and cross-stream velocity are shown in Figs. 8(a)-(c).

From a collection of u'_f -data as in Figs. 7 and 8, the penetration height of SJCF is now examined. In Fig. 9(a), y_{max} data for a number of cases are shown as a function of the stroke length. The parameters for each of the curves are indicated in the legend. Clearly, y_{max} is not a unique function of L_0/D and depends on other parameters. The penetration of a steady jet-in-cross-flow (JICF) is a function of the momentum-flux ratio that, for incompressible flow, is equal to the square of the jet-to-cross-stream velocity ratio. Following that observation, the data of Fig. 9(a) are first plotted as a function of $(V_0/U_\infty)^2$ in Fig. 9(b). Also shown in Fig. 9(b) is the correlation for the penetration of a JICF (see, e.g., Ref. 24):

$$\frac{y_{max}}{D} = \left(\frac{x}{D} \right)^{0.33} J^{0.43}, \quad (4)$$

where J is substituted by $(V_0/U_\infty)^2$. It is clear that the curves for the SJCF have collapsed, however, they are not represented well by Eq. 4. When the same data are viewed as a function of $(V_{max}/U_\infty)^2$ not only a reasonable collapse occurs but also there is close agreement with Eq. 4. This can be seen in Fig. 9(c). Thus, the SJCF trajectory is predicted by the correlation equation of a JICF when the momentum-flux ratio for the former is defined as $J = (V_{max}/U_\infty)^2$. It should be borne in mind that the definitions for J as well as y_{max} are intrinsically different for a JICF; J equals $(V_{jet}/U_\infty)^2$ and y_{max} denotes the distance of the location of maximum U from the wall. Nevertheless, the applicability of Eq. 4 to SJCF underscores another similarity of the synthetic jet with a steady jet when subjected to a cross-flow.

The applicability of Eq. 4 to the trajectory of a SJCF is further explored. First, u'_f -profiles at different downstream locations along the tunnel centerline are presented in Figs. 10 (a)-(b) for cases 8 and 6 of Table 1. The variations of the penetration height y_{max} are shown in Fig. 11. The symbols represent data, the broken lines are curve-fit through the data, while the solid lines indicate predictions of Eq. 4. It is clear that with the chosen definitions the trajectories of a SJCF and a JICF, for the ranges of Stokes and Reynolds numbers covered, are practically identical.

Finally, sample time-averaged data for a selected SJCF ($L_0/D = 19.9$ and $J = 5.95$, case 8 of Table 1) are shown in Figs. 12 and 13. Cross-sectional distributions of mean velocity, mean streamwise vorticity and turbulence intensity measured at $x/D = 5$ are presented in Figs. 12(a)-(c), respectively. Mean velocity contours in Fig. 12(a) exhibit a 'dome' of low-momentum fluid. A counter-rotating pair of vortices can be seen in Fig. 12(b). The data in Fig. 12(c) reveal the vigorous turbulent activity and the momentum exchange between the boundary layer and the cross-stream. These characteristics are similar to that of a JICF. Some differences, however, may be noted. Unlike with a JICF, another pair of counter-rotating vortices is observed near the wall in Fig. 12(b). The mean velocity data (Fig. 12a) does not show the typical 'kidney-shaped' structure of high momentum fluid over the dome of boundary layer fluid.

The downstream evolution of the SJCF is shown in Fig. 13 with mean velocity distributions for indicated x/D locations. The characteristic kidney-shape of a

JICF is detected only near the orifice in Fig. 13(a). With increasing downstream distance the higher momentum fluid spills on the sides and the distribution is marked by only the dome of low-momentum boundary layer fluid. As noted before, this is in contrast to a JICF where velocity overshoot at high momentum-flux ratios is considerable and persists far downstream.²⁵ The details of the unsteady flow dynamics leading to the observed flowfield evolution and the steady vortex pairs seen in Fig. 12(b) will be addressed in Part 2 of the paper.

CONCLUSIONS

Results of an experimental investigation on synthetic jets from round orifices with and without cross-flow are presented. The main conclusions are enumerated in the following. (1) For the parameter range covered, the threshold for the formation of synthetic jet without cross-flow is about $L_0/D = 0.5$. A SJ is not formed at lower L_0/D . The result is in agreement with observations made in Ref. 4. (2) There appears to be an upper threshold of about $L_0/D = 10$ above which the profiles of normalized centerline mean velocity become invariant. This upper threshold may have a connection with the phenomenon of saturation of impulsively generated vortices observed in Ref. 23. (3) For a given frequency and U_∞ , the penetration height y_{max} of a SJCF increases with increasing stroke length, L_0/D . However, unlike various other properties, y_{max} is not a function of L_0/D . (4) It is found that y_{max} at a given x solely depends on the momentum-flux ratio. For the present incompressible flow, when this ratio is defined as $J = (V_{max}/U_\infty)^2$, not only all the penetration height data collapse but also the trajectories are predicted well by correlation equations for steady jets-in-cross-flow. (5) Mean velocity, streamwise vorticity as well as turbulence intensity distributions for a SJCF are found to be similar to those of a steady JICF. A pair of counter-rotating streamwise vortices, resembling the 'bound vortex pair' of a JICF, is clearly observed. Mean velocity distributions exhibit the dome of low momentum fluid pulled up from the boundary layer. The entire domain is characterized by high turbulence intensity.

ACKNOWLEDGEMENTS

The work was supported by NASA-OAI Collaborative Aerospace Research and Fellowship Program. The second author is grateful to Connecticut Space Grant College Consortium—EPSCoR Core Funding for providing support. The authors are also thankful to Dr. Gerard E. Welch of US Army for valuable inputs.

REFERENCES

- ¹Smith, B. L., and Glezer, A., "The Formation and Evolution of Synthetic Jets," *Phys. Fluids*, 10 (9): 2281-2297, 1998.

- ²Ingard, U. and Labate, S., "Acoustic Circulation Effects and the Nonlinear Impedance of Orifices," *J. Acous. Soc. Am.*, 174 (1): 211-218, 1950.
- ³Lighthill, M.J., "Acoustic Streaming," *J. Sound & Vibration*, 61(3), 391-418, 1978.
- ⁴Utturkar, Y., Holman, R., Mittal, R., Carroll, B., Sheplak, M., and Cattafesta, L., "A Jet Formation Criterion for Synthetic Jet Actuators," AIAA Paper 2003-0636, 41st Aerospace Sciences Meeting and Exhibit, Reno, NV, January 2003.
- ⁵Carter, J. and Soria, J., "The Evolution of Round Zero-Net-Mass-Flux Jets," *J. Fluid Mech.*, 472: 167-200, 2002.
- ⁶Bera, J. C., Michard, M., Grosjean, N., and Comte-Bellot, G., "Flow Analysis of Two-Dimensional Pulsed Jets by Particle Image Velocimetry," *Exp. Fluids*, 31: 519-532, 2001.
- ⁷Smith, B. L. and Swift G. W., "A Comparison Between Synthetic Jets and Continuous Jets," *Exp. Fluids*, DOI 10.1007/s00348-002-0577-6
- ⁸Smith, D. R., Amitay, M., Kibens, Parekh, D. E., and Glezer, A., "Modification of Lifting Body Aerodynamics Using Synthetic Jet Actuators," AIAA Paper 98-0209, 36th AIAA Aerospace Sciences Meeting and Exhibit, Reno, NV, January 1998.
- ⁹Amitay, M., Smith, B. L., and Glezer A., "Aerodynamic Flow Control Using Synthetic Jet Technology," AIAA Paper 98-0208, 36th AIAA Aerospace Sciences Meeting and Exhibit, Reno, NV, January 1998.
- ¹⁰Amitay, M., Kibens, V., Parekh, D. E., and Glezer, A., "Flow Reattachment Dynamics over a Thick Airfoil Controlled by Synthetic Jet Actuators," AIAA Paper 99-1001, 37th AIAA Aerospace Sciences Meeting and Exhibit, Reno, NV, January 1999.
- ¹¹Amitay, M., Smith, D. R., Kibens, V., Parekh, D. E., and Glezer, A., "Modification of the Aerodynamics Characteristics of an Unconventional Airfoil Using Synthetic Jet Actuators," *AIAA Journal*, 39 (3): 361-370, 2001.
- ¹²Honohan, A. M., Amitay, M., and Glezer, A., "Aerodynamic Control Using Synthetic Jets," AIAA Paper 2000-2401, AIAA Fluids Meeting, Denver, CO, 2000.
- ¹³Smith, B. L., and Glezer, A., "Jet Vectoring Using Synthetic Jets," *J. Fluid Mech.*, 458:1-34, 2002.
- ¹⁴Amitay, M., Honohan, A., Trautman, M., and Glezer, A., "Modification of the Aerodynamic Characteristics of Bluff Bodies Using Fluidic Actuators," AIAA Paper 97-2004, 28th AIAA Fluid Dynamics Conference, Snowmass, CO, June 1997.
- ¹⁵Chen, Y., Liang, S., Aung, K., Glezer, A., Jagoda, J., "Enhanced Mixing in a Simulated Combustor Using Synthetic Jet Actuators," AIAA Paper 99-0449, 37th Aerospace Sciences Meeting and Exhibit, Reno, NV, January 1999.
- ¹⁶Amitay, M., Pitt, D., Glezer, A., "Separation Control in Duct Flows," *Journal of Aircraft*, 39 (4): 616-620, 2002.
- ¹⁷Liu, Z., Sankar, L. N., Hassan, A. A., "Alteration of the Tip Vortex Structure of a Hovering Rotor Using Oscillatory Jet Excitation," AIAA Paper 99-0906.
- ¹⁸McCormack, D.C., "Boundary layer separation control with directed synthetic jets," AIAA Paper 2000-0519, 38th Aerospace Sciences Meeting, Reno, NV, January, 2000.
- ¹⁹Gilarranz, J.L., Traub, L.W. and Rediniotis, O.K., "Characterization of a compact, high-power synthetic jet actuator for flow separation control", AIAA Paper 2002-0127, 40th Aerospace Sciences Meeting, Reno, NV, January, 2002.
- ²⁰Grossman, K., Bohdan, C. and Vanwie, D., "Sparkjet actuators for flow control", AIAA Paper 2003-0057, 41th Aerospace Sciences Meeting, Reno, NV, January, 2003.
- ²¹Anderson, J.S., "The effect of an air flow on a single side branch Helmholtz resonator in a circular duct", *J. Sound & Vib.*, 52(3), pp. 423-431, 1977.
- ²²Smith, B., Trautman, M., and Glezer, A., "Controlled Interactions of Adjacent Synthetic Jets," AIAA Paper 99-0669, 1999.
- ²³Gharib, M., Rambod, E., and Shariff, K., "A Universal Time Scale for Vortex Ring Formation," *J. Fluid Mech.*, 360: 121-140, 1998.
- ²⁴Zaman, K. B. M. Q., and Foss, J. K., "The Effect of Vortex Generators on a Jet in a Cross-Flow," *Phys. Fluids*, 9 (1): 106-114, 1997.
- ²⁵Milanovic, I. M., and Zaman, K. B. M. Q., "Highly Inclined Jets in Cross-Flow," AIAA Paper 2003-183, 41st Aerospace Sciences Meeting and Exhibit, Reno, NV, January 2003.

Table 1 Initial condition for different SJ Configurations.

Case	D (in)	f (Hz)	A (Vrms)	V_0	L_0/D	Re	Re/S^2
1	0.75	12.5	0.67	1.0	1.3	811	0.42
2	0.75	12.5	2.3	5.4	6.9	4,311	2.21
3	0.75	12.5	5.8	16.6	21.3	13,236	6.78
4	0.75	12.5	9.6	23.0	29.4	18,307	9.37
5	0.75	25	0.67	3.2	2.1	2,586	0.66
6	0.75	25	2.3	11.7	7.5	9,331	2.39
7	0.75	25	5.8	22.5	14.4	17,952	4.60
8	0.75	25	9.6	31.1	19.9	24,747	6.34
9	0.75	50	0.67	1.3	0.4	1,065	0.14
10	0.75	50	2.3	4.5	1.4	3,601	0.46
11	0.75	50	4.6	9.9	3.2	7,911	1.01
12	0.75	50	9.6	24.3	7.8	19,372	2.48
13	0.75	118	6	5.0	0.7	3,956	0.21
14	0.375	25	9.6	27.5	35.1	10,928	11.19
15	1.5	38	9.6	26.1	5.5	41,584	1.75
16	3	65	2.3	5.1	0.3	16,228	0.10
17	3	65	9.6	14.4	0.9	45,844	0.28

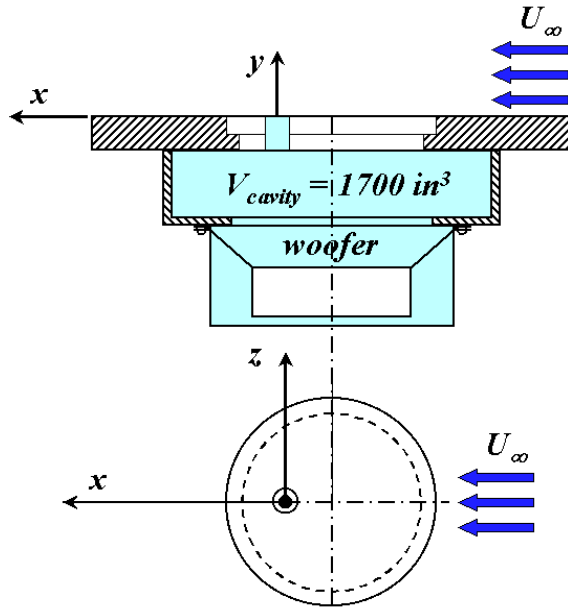


Fig. 1 Experimental setup and orifice configuration.

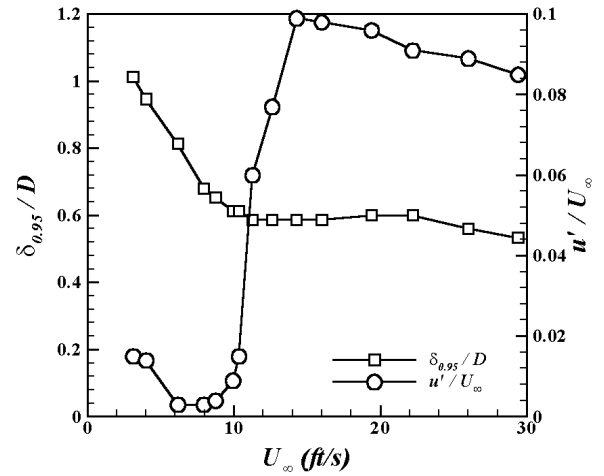


Fig. 2 Approach boundary layer characteristics. Boundary layer thickness is measured at $x/D = -0.5$ and $z/D = 2$. Turbulence intensity data are for the fixed height, $y/D = 0.15$. ($D = 0.75''$).

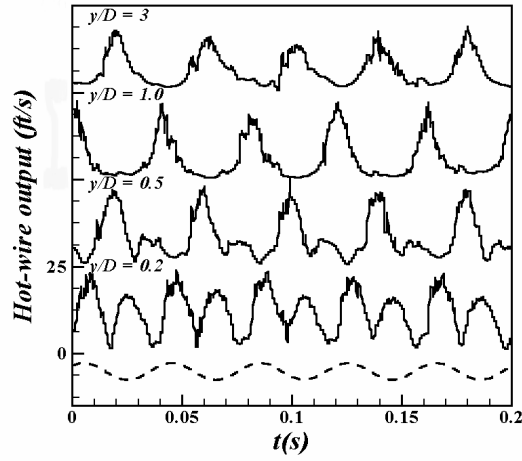


Fig. 3 Hot-wire output at various vertical locations for $D = 0.75''$ orifice; $x/D = 0$, $z/D = 0$, $f = 25$ Hz, $A = 9.6$ V, $U_\infty = 0$. Dashed curve represents sample of signal fed to the woofer.

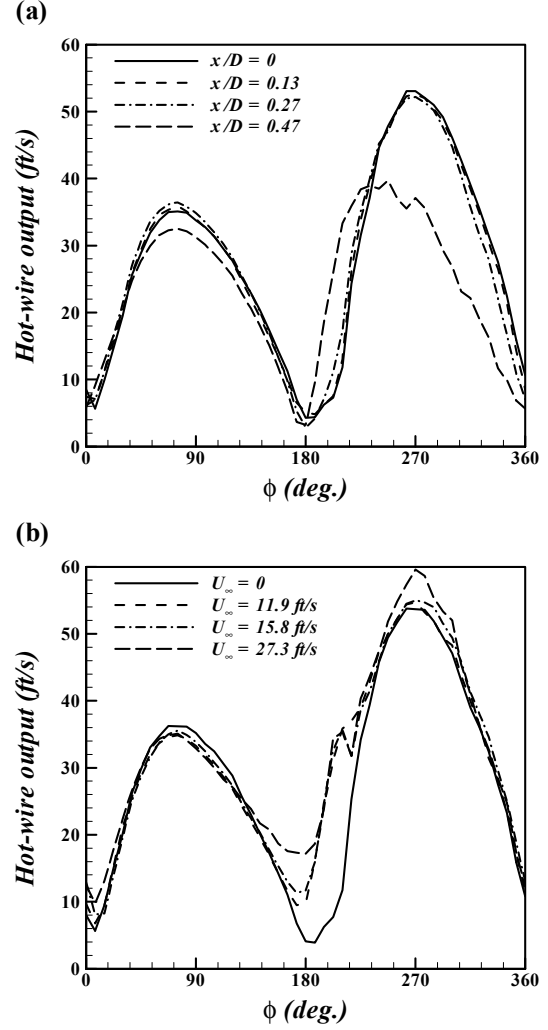


Fig. 4 Phase-averaged hot-wire output at exit of $D = 0.75''$ orifice; probe at $y/D = 0.2$, $z/D = 0$, and $f = 25$ Hz, $A = 9.6$ V for all cases. (a) Measurements at indicated radial (x/D) locations with $U_\infty = 0$; (b) Measurements at $x/D = 0$ for indicated values of U_∞ .

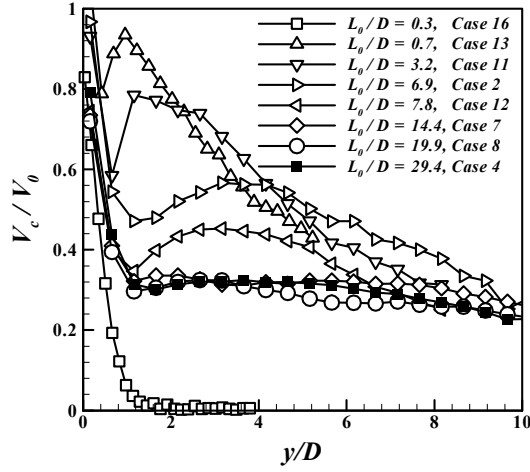


Fig. 5 Normalized centerline velocity profiles for SJ's without cross-flow ($U_\infty = 0$); $x/D = 0$, $z/D = 0$. Cases refer to Table 1.

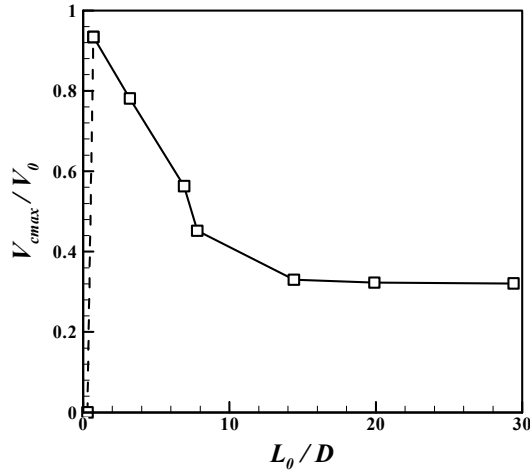


Fig. 6 Peak values of mean velocity (V_c) on the axis of SJ without cross-flow versus L_0/D corresponding to the data of Fig. 5.

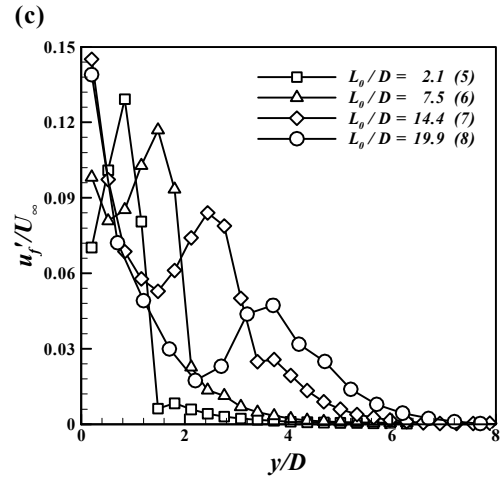
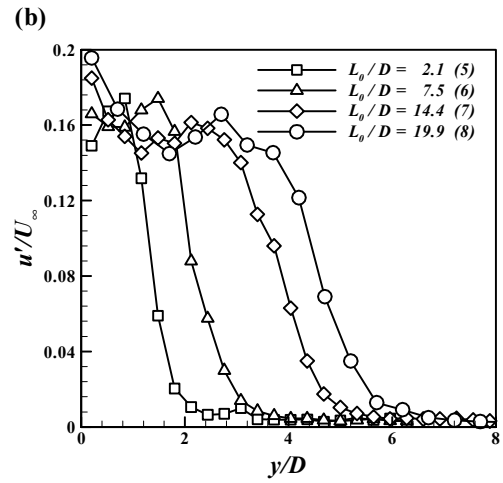
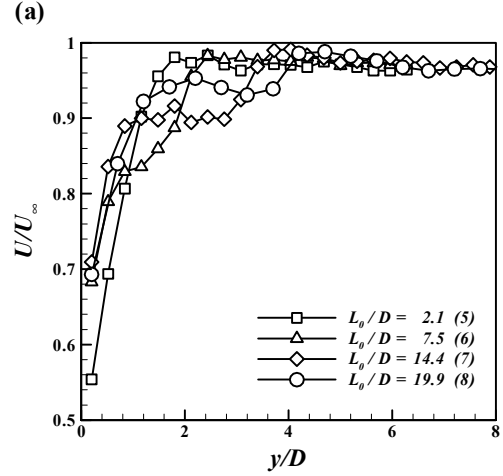


Fig. 7 Mean and fluctuating velocity profiles for SJCF; $x/D = 5$, $z/D = 0$, $f = 25$ Hz, $U_\infty = 20$ ft/s. Numbers in parentheses represent case numbers of Table 1. (a) Mean velocity, (b) Turbulence intensity, (c) Fundamental (r.m.s.) intensity.

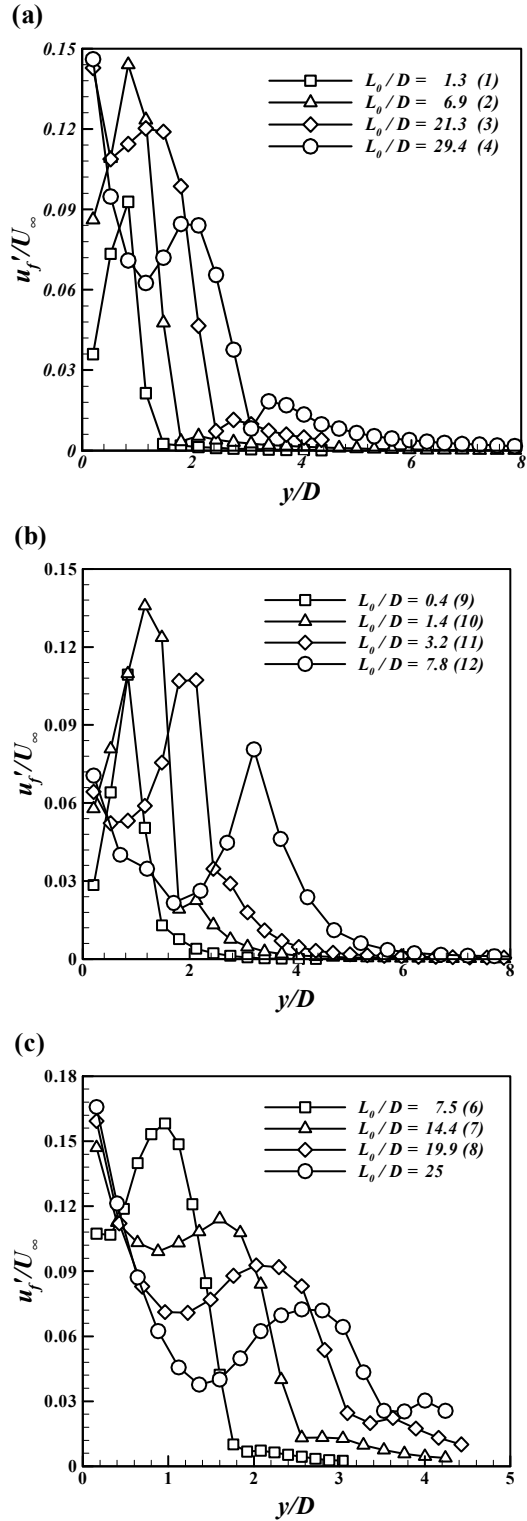


Fig. 8 Profiles of fundamental (r.m.s.) intensity at $x/D = 5$, $z/D = 0$. Numbers in parentheses represent case numbers of Table 1. (a) $f = 12.5$ Hz, $U_\infty = 20$ ft/s, (b) $f = 50$ Hz, $U_\infty = 20$ ft/s, (c) $f = 25$ Hz, $U_\infty = 27.3$ ft/s.

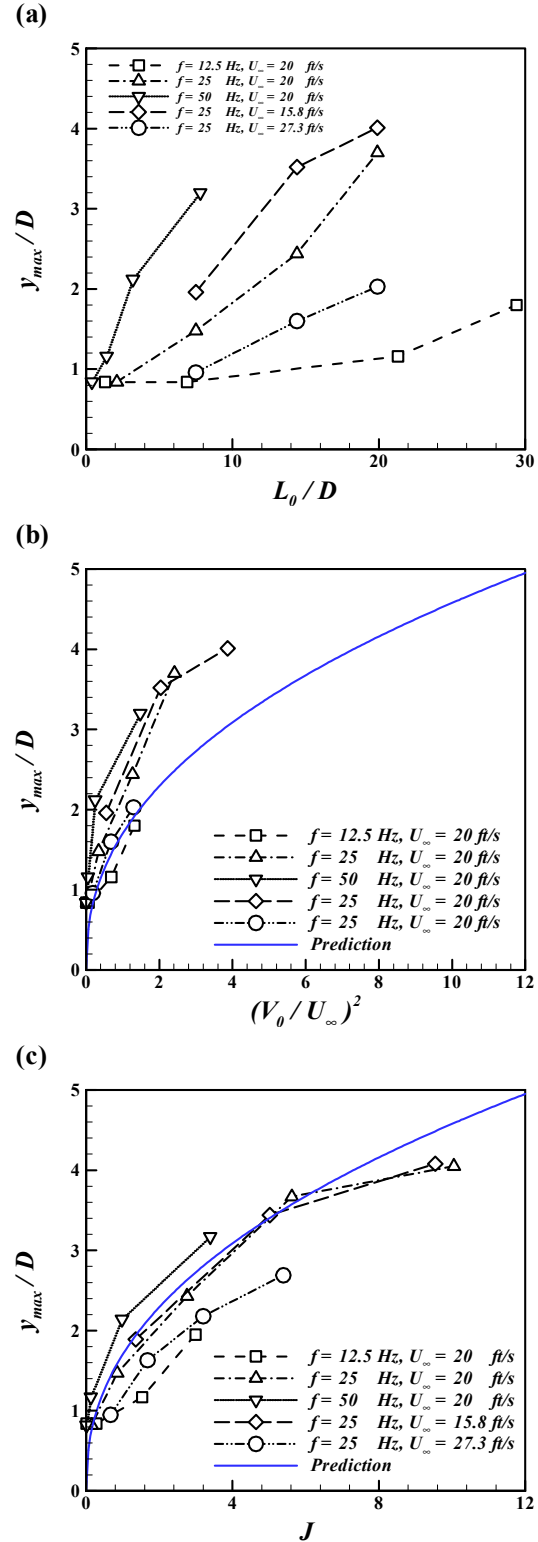


Fig. 9 Vertical location of peak- u_f' as a function of (a) stroke length, L_0/D , (b) $(V_0/U_\infty)^2$, (c) $J = (V_{max}/U_\infty)^2$; $x/D = 5$, $z/D = 0$, $U_\infty = 20$ ft/s.

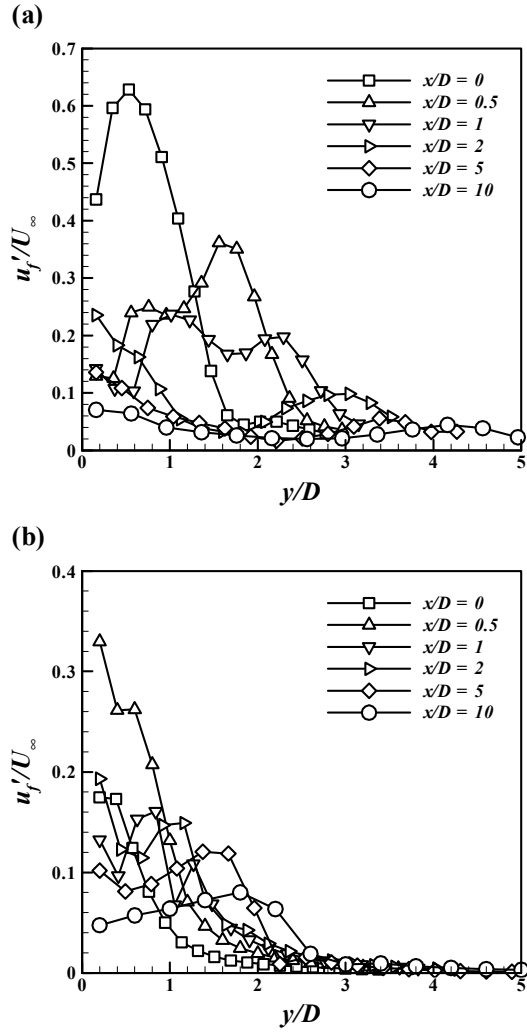


Fig. 10 Vertical profiles of fundamental (r.m.s.) intensity at different downstream locations; $z/D = 0$, $f = 25$ Hz, $U_\infty = 20$ ft/s. (a) $L_0/D = 19.9$ (8), $J = 5.95$, (b) $L_0/D = 7.5$ (6), $J = 0.85$.

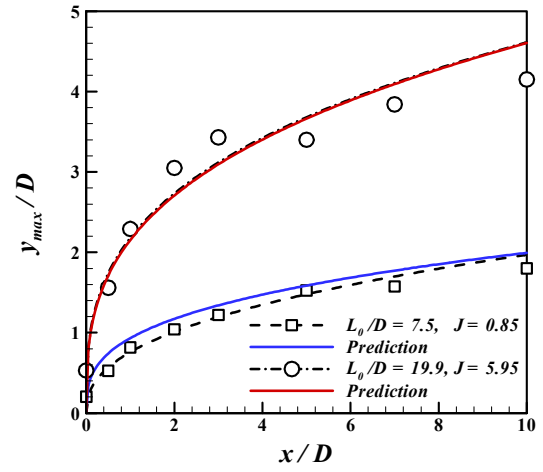


Fig. 11 'SJ trajectory' based on peak- u'_f locations; $z/D = 0$, $f = 25$ Hz, $U_\infty = 20$ ft/s.

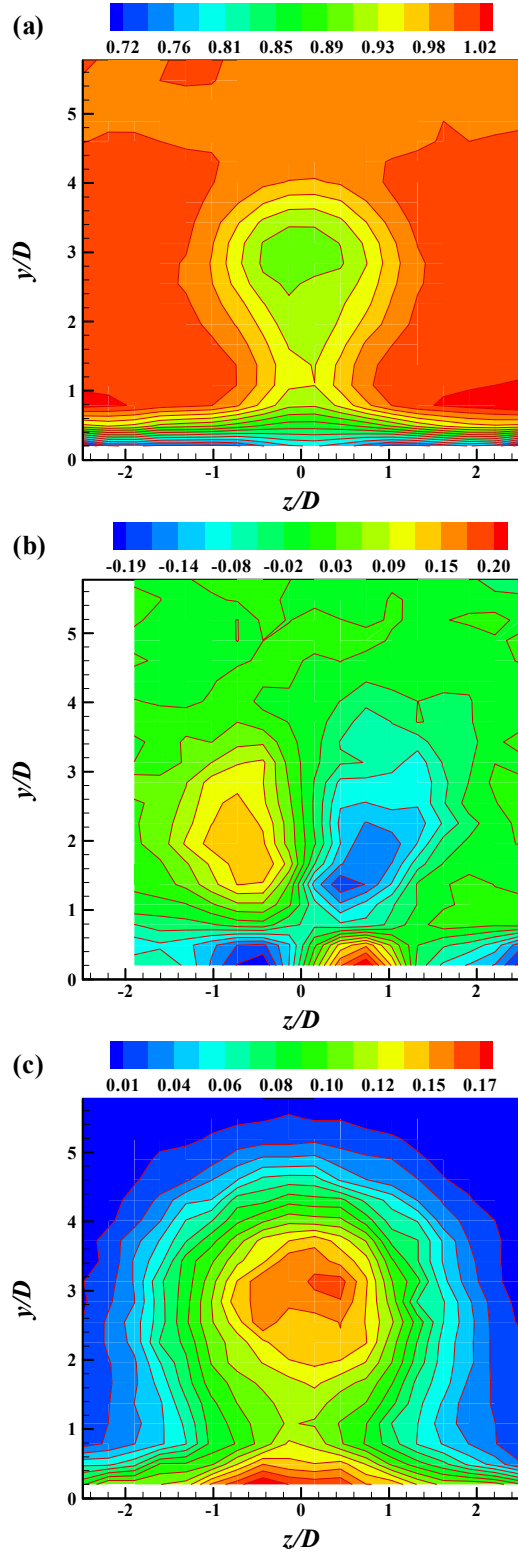


Fig. 12 Contours of streamwise (a) mean velocity, (b) vorticity and (c) turbulence intensity for SJCF; $x/D = 5$, $f = 25$ Hz, $U_\infty = 20$ ft/s, $L_0/D = 19.9$ (8).

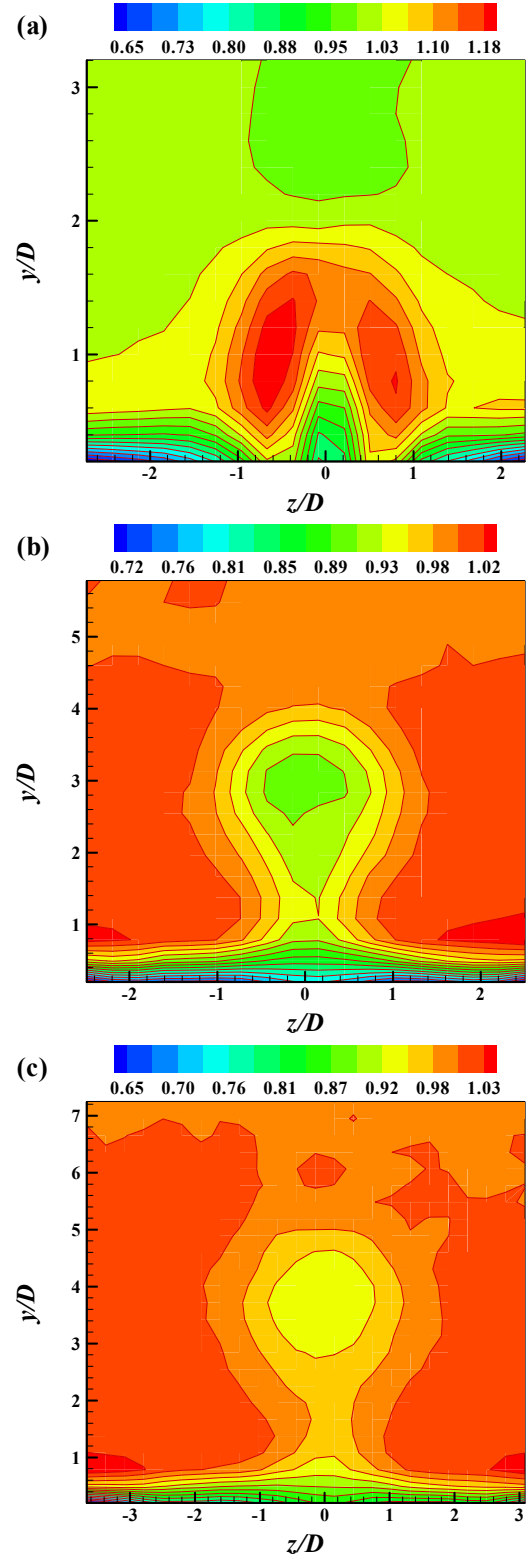


Fig. 13 Downstream development of streamwise mean velocity for SJCF of Fig. 12. (a) $x/D = 0.5$, (b) $x/D = 5$, (c) $x/D = 10$.